

Unified percolation scenario for the α and β processes in simple glass formers

Liang Gao, Hai-Bin Yu*

Wuhan National High Magnetic Field Center and School of Physics,
Huazhong University of Science and Technology, Wuhan 430074, Hubei, China

Thomas B. Schröder, Jeppe C. Dyre†

Glass and Time, IMFUFA, Department of Science and Environment,
Roskilde University, P.O. Box 260, DK-4000 Roskilde, Denmark

(Dated: November 15, 2024)

Given the vast differences in interaction details, describing the dynamics of structurally disordered materials in a unified theoretical framework presents a fundamental challenge to condensed-matter physics and materials science. This paper investigates numerically a percolation scenario for the two most important relaxation processes of supercooled liquids and glasses. For nine binary glass formers we find that, as temperature is lowered from the liquid state, percolation of immobile particles takes place at the temperature locating the α process. Mirroring this, upon continued cooling into the glass, mobile-particle percolation pinpoints a Johari-Goldstein β relaxation whenever it is well separated from the α process. For 2D systems under the same conditions, percolation of mobile and immobile particles occurs nearly simultaneously and no β relaxation can be identified. Our findings suggest a general description of glassy dynamics based on a percolation perspective.

I. INTRODUCTION

When subjected to an external disturbance, a glass-forming liquid relaxes extremely slowly toward equilibrium [1–10]. Depending on the temperature the main so-called α relaxation time, τ_α , can be seconds, hours, even months, with no other limit than the patience of the experimentalist [2–5, 9–11]. In the Maxwell model of viscoelasticity [5, 12], glass-forming liquids behave like a solid on time scales much shorter than τ_α and flow on much longer time scales. Interestingly, most such liquids exhibit additional, faster relaxations. The most prominent one is the Johari-Goldstein β process, which is observed in virtually all glass-forming organic liquids, polymers, metallic glasses, etc [13–17]. It was known already in the 1960s that polymers also exhibit relaxation processes above the α relaxation frequency $\sim 1/\tau_\alpha$. These were attributed to side-chain motions [13], and it was therefore a great surprise when Johari and Goldstein in 1970 reported fast processes also in glasses of small rigid molecules [18]. To explain this they proposed the existence of “islands of mobility” in which what became known as the Johari-Goldstein β relaxation takes place [18, 19]. This constituted an early indication of the dynamic heterogeneities that were later recognized as universal in glass-forming liquids [6, 20, 21].

Research in the past decades has demonstrated that β relaxation plays a crucial role for the mechanical and thermal properties of amorphous materials [22]. Ngai has suggested that the β process is a precursor of the main α relaxation: before the onset of β relaxation one finds a regime in which molecules are confined to cages

defined by the anharmonic intermolecular potential [23–25]. A related idea was discussed in 1999 by Kudlik *et al.*, who proposed that the β process in molecular liquids is a local, spatially restricted reorientation process preceding the α relaxation [26], reminiscent of the fundamental prediction of mode-coupling theory [27]. Experiments have confirmed the caged-molecule picture of the β process by the detection of small-angle jumps [28], but interestingly large-angle jumps are sometimes also involved in β relaxation [29].

Although most papers on the β process report results for the glass phase, β relaxation is present also in the equilibrium metastable liquid phase above the glass-transition temperature T_g . In many cases, however, β relaxation is here partly merged with the α process and observed only as an excess wing of the latter [30–33]. Long-time annealing may separate the β relaxation from the excess wing to establish it as an independent, well-defined process [31]. In other cases, however, annealing *annihilates* the β process by decreasing its magnitude to below the resolution limit [34].

Like any liquid a glass-forming liquid is disordered so it is reasonable to assume that the flow-event energy barriers at any given time vary more or less randomly in space. This amounts to replacing complexity by randomness, an old and venerated strategy of simplification [35]. Once spatial randomness is introduced, the phenomenon of percolation comes into mind connecting *randomness* and *geometry* [36–39]: If finite-sized domains in space are marked randomly one after the other, at some point the marked clusters will percolate throughout the sample. The value of the percolation threshold depends on the spatial dimension and the specific model in question. In one dimension the percolation threshold is unity. On a 2d cubic lattice the link-percolation threshold is 50% by self-duality [37–39]. For $d > 2$ the percolation threshold decreases and for $d \rightarrow \infty$ it approaches zero. The perco-

* haibinyu@hust.edu.cn

† dyre@ruc.dk

lation threshold is 0.25 for link percolation on a 3d cubic lattice and 0.31 for site percolation on the same lattice [37–39].

Recently a double-percolation picture was proposed linking the α and β processes to the percolation of immobile and mobile regions, respectively [40] (Fig. 1(a)). Associating a given energy barrier, ΔE , with a relaxation time $\propto \exp(\beta\Delta E)$, the “minimax” idea is that τ_α is controlled by the lowest energy barriers on the percolation cluster that is formed by the most immobile regions, i.e., those of the largest barriers. On time scales longer than τ_α the immobile-region percolation cluster breaks up and the system can no longer sustain an overall shear stress. This makes flow possible because the rigid solid-like structure, which maintains the energy barriers throughout the sample by keeping surrounding molecules in place, disappears on time scales longer than τ_α . As a consequence, the largest energy barriers are never overcome, hence their light color in Figure 1(a). Borrowing a term from NMR [41, 42] this phenomenon was initially referred to as “exchange”; nowadays it is often termed “facilitation” [43–49].

On very short time scales, only the lowest-barrier regions are relevant. These are spatially separated. Extended fast motion becomes possible when regions of longer time scales percolate, which gives rise to a new relaxation channel identified with the β process [50, 51].

The conception that percolation is important for understanding relaxations in glass-forming liquids and glasses has a long history [40, 50–64]. A double-percolation picture related to the above was proposed in 1996 by Novikov *et al.* in the context of percolation of liquid-like and solid-like domains defined by the largest and smallest vibrational mean-square displacement, respectively [65], but no relation to the α and β processes was proposed at the time.

The present paper tests the double-percolation scenario by extensive computer simulations of binary models in two and three dimensions. We find that whenever the α and β processes are well separated, they correspond to the percolation of immobile and mobile particles, respectively, confirming the double-percolation scenario. There are also cases where the two processes are not well separated, however; in particular this is always the case in 2d.

II. RESULTS

Figure 1 illustrates our main idea and how it is tested in simulations. Figure 1(a) presents the double-percolation scenario by considering a generic linear-response loss, $\chi''(\omega)$, as a function of the angular frequency ω for an equilibrium glass-forming liquid (lower panel). The system is assumed to have an activation-energy distribution much wider than $k_B T$, which constitutes a highly idealized situation. Such a clear separation of the α and β processes is not often seen in experi-

ments on equilibrium glass-forming liquids and would be extremely difficult to test in simulations of an equilibrium supercooled liquid. To address this issue, we adopt the strategy of Ref. 51 mimicking experimental dynamic mechanical spectroscopy (DMS) by occasionally, during a slow cooling through the glass transition, subjecting the sample to a periodic deformations to probe the dynamic shear modulus. The point is that, although the schematic picture in Fig. 1(a) refers to the equilibrated liquid, mobile- and immobile-region percolation occurs also as the system falls out of equilibrium going below T_g . The only difference is that here the immobile regions freeze and their percolation cluster becomes permanent, while in the equilibrium liquid this cluster changes continuously (on the τ_α time scale).

In DMS the glass transition is seen as a maximum in a plot of the temperature dependence of a fixed-frequency mechanical loss while the β relaxation manifests itself as a second smaller peak below T_g . Figure 1(b) illustrates our simulation procedure. At selected times during the cooling, the sample of 32000 particles is subjected to a periodic elongation of 1.4% while the two transverse dimensions are decreased by 0.7%. This results in a periodic stress on a constant-volume sample, the magnitude and phase of which determine the complex frequency-dependent shear modulus $G(\omega)$ (details are given in the Supplementary Material). The right side of panel (b) shows an example of $G(\omega) = G'(\omega) + iG''(\omega)$ at three frequencies, plotted as a function of temperature during cooling where squares and circles give the real and imaginary parts of $G(\omega)$, respectively. Not surprisingly, the β process is most clearly visible at the lowest frequency (upper panel).

There is a considerable freedom in how to define mobile and immobile particles. In order not to introduce arbitrary parameters we proceeded as follows (Fig. 1(c)). For a given time interval Δt , mobile particles are defined via the (all-particle) van Hove function $p(u, \Delta t)$. Particles with displacement larger than the first minimum of $p(u, \Delta t)$ are designated as “mobile”, all other particles as “immobile”. This of course depends on Δt , which we put equal to $2\pi/\omega$ of the mechanical deformation in question. Having thus divided the particles into two classes, mobile/immobile particles, two particles of the same type are designated to belong to the same cluster if their distance is smaller than the minimum of the (all-particle) radial distribution function, $g(r)$, compare the lower panel of Fig. 1(c). One can now identify the largest cluster (LC) and the second-largest cluster (SLC) of the mobile and the immobile particles respectively at any time during the cooling, compare Figs. 1(d)-(f). In summary, at any given time during the cooling the frequency in question defines a time scale used to classify particles into mobile and immobile, and each of these two classes are subdivided into clusters.

Figures 2(a), (b), and (c) show the results of this procedure for a $\text{Ni}_{80}\text{P}_{20}$ mixture cooled through the glass transition at the three frequencies of Fig. 1. (a) gives re-

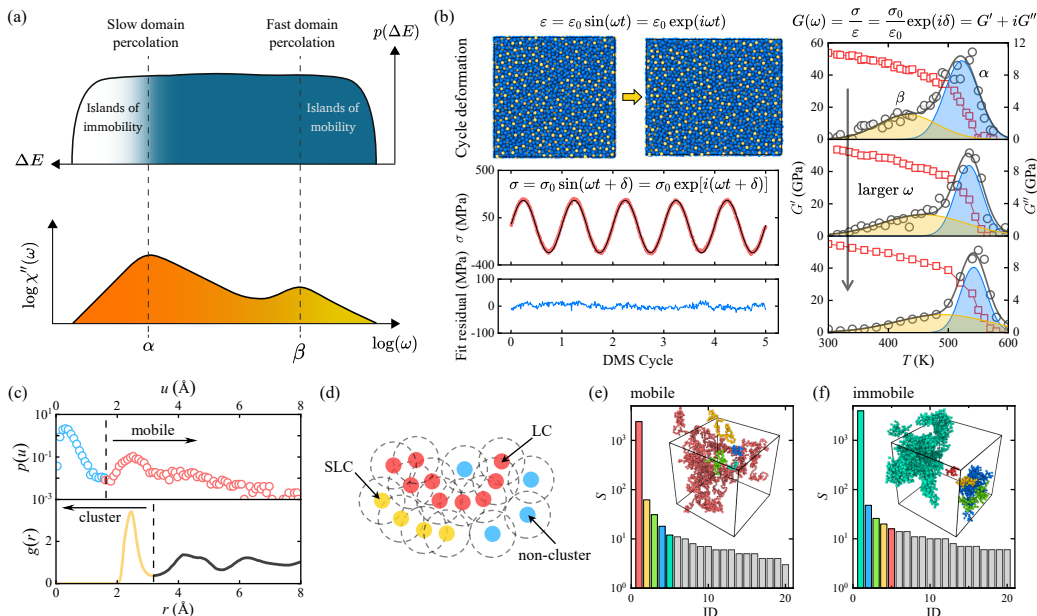


FIG. 1. Main concepts. (a) Double-percolation scenario for a glass-forming liquid’s equilibrium linear-response properties, assuming the activation-energy distribution is much wider than $k_B T$. On a certain time scale the low-activation-energy “islands of mobility” percolate, opening a relaxation channel identified with the Johari-Goldstein (JG) β relaxation [50, 51]. A much larger time scale characterizes the percolation of the high-activation-energy “islands of immobility” that locate the α process [40]. (b) Molecular Dynamics simulations mimicking experimental Dynamic Mechanical Spectroscopy for a $\text{Ni}_{80}\text{P}_{20}$ mixture. At selected times during a cooling through the glass transition, the sample is deformed periodically to determine the dynamic shear modulus $G(\omega)$. (c) Definition of mobile particles on the time scale $\Delta t = 2\pi/\omega$. The upper panel shows the distribution of all-particle displacements, the van Hove function $p(u, \Delta t)$. Particles with displacement larger than its minimum are designated as mobile, the remaining ones as immobile. The lower panel shows the all-particle radial distribution function $g(r)$. Whenever two mobile/immobile particles are closer than the first $g(r)$ minimum, they belong by definition to the same cluster [66]. (d) Example of the largest-particle cluster (LC) and second-largest-particle cluster (SLC) defined separately for mobile and immobile particles. (e) and (f) show examples of mobile and immobile particle clusters (insets) and their size (S) histograms.

sults for the lowest frequency where the α and β processes are best separated, (b) and (c) give results for higher frequencies. The upper panels show the shear-mechanical loss modulus as a function of temperature during the cooling. The lower panels show the fraction of particles belonging to the LC (orange and green diamonds) and SLC (yellow and blue circles) of mobile (left) and immobile (right) particles. The two dashed vertical lines mark the percolation temperatures T_{P_m} and $T_{P_{im}}$ defined by the criterion that LC is 100 times larger than the SLC.

Focusing first on the immobile particles, for all three frequencies simulated we find that during cooling the LC and SLC fractions are virtually identical down to a temperature slightly above that of the α peak, below which LC completely dominates. This is where the immobile particles percolate. Upon continued cooling into the glass phase a mirror phenomenon is found for the β peak: The LC and SCL fractions are quite different down to a temperature slightly below that of the β peak, at which point all mobile-particle clusters become small ($\sim 1\%$). This shows that the β process is characterized by mobile-particle percolation [51, 58]. In summary, the α peak is found where the immobile particles percolate and the β

peak is found where the mobile particles percolate.

To investigate the generality of these findings we carried out simulations of four other metallic glasses, $\text{Al}_{90}\text{Sm}_{10}$, $\text{Al}_{85}\text{Sm}_{15}$, $\text{Ni}_{65}\text{Nb}_{35}$, and $\text{Cu}_{50}\text{Zr}_{50}$, as well as of the Kob-Andersen binary Lennard-Jones mixture [67] (Fig. 2 and Fig. 3). The results can be summarized as follows: 1) In all cases the α process is characterized by immobile-particle percolation; 2) Whenever there is a well-defined β process, it is characterized by mobile-particle percolation (Fig. 2); 3) For the Kob-Andersen, $\text{Ni}_{65}\text{Nb}_{35}$, and $\text{Cu}_{50}\text{Zr}_{50}$ models, the β process is not well separated from the α process and merely visible as an excess wing of the latter (Fig. 3).

What is the difference between the systems of Fig. 2 with a clearly visible β relaxation and those of Fig. 3 with only an excess wing? Whenever the mobile- and immobile-particle percolation temperatures are close, one cannot expect to find well separated α and β relaxations. Since α is the main relaxation, this means that the β process will only be an excess wing of the α . The percolation temperatures are reported in Table I (note that these by definition depend on the frequency / time scale in question). The table reveals a threshold of $T_{P_m}/T_{P_{im}} \cong 0.85$

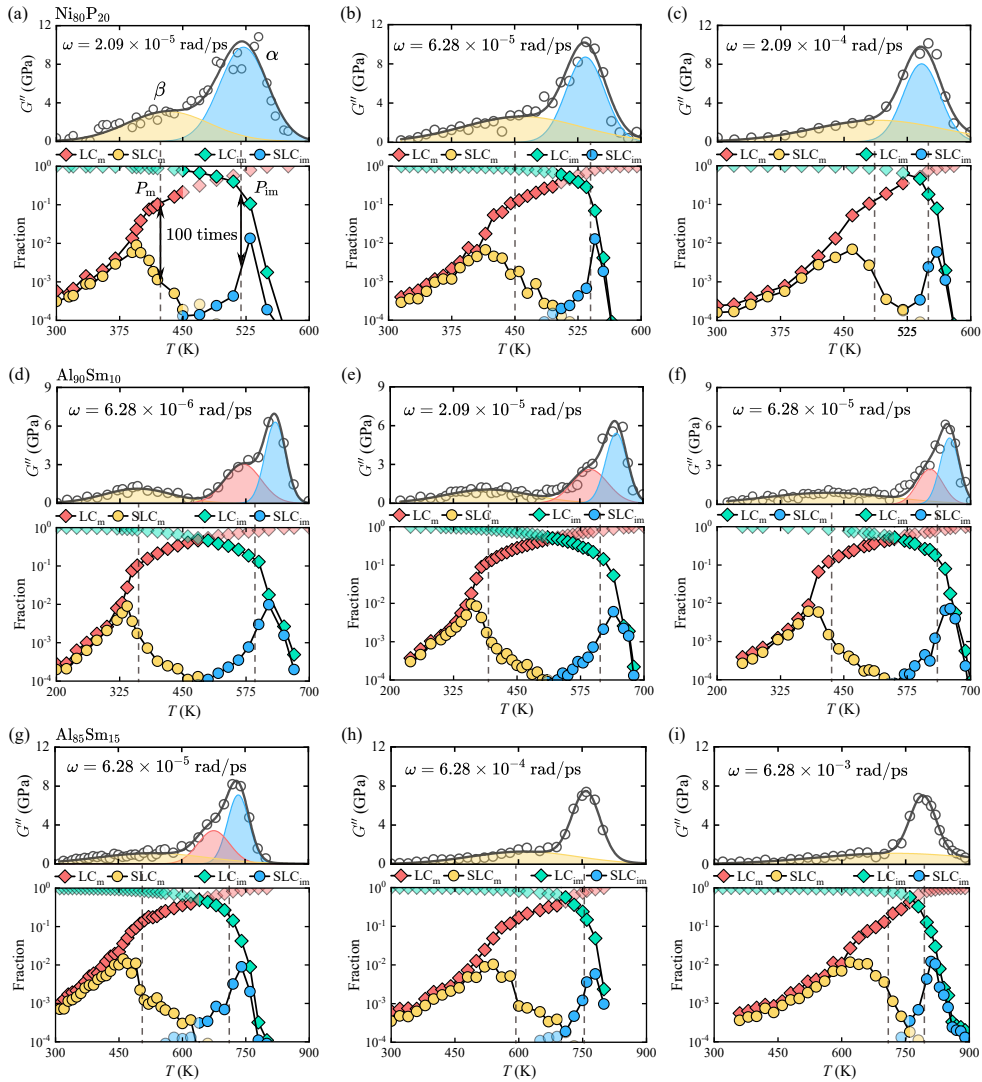


FIG. 2. Double-percolation cluster analysis of $\text{Ni}_{80}\text{P}_{20}$, $\text{Al}_{90}\text{Am}_{10}$, and $\text{Al}_{85}\text{Sm}_{15}$ mixtures at different frequencies. For each subfigure the upper panel displays the shear-mechanical loss modulus $G''(\omega)$ monitored regularly during a cooling at 0.1 K/ns. The loss modulus is fitted to a sum of Gaussian peaks, corresponding to α (blue), α_2 reflecting the α process asymmetry [40] (pink, not needed in all spectra), and β (yellow) processes. The lower panels show the fraction of particles belonging to the largest cluster (LC) (orange/green) and the second-largest cluster (SLC) (yellow/blue) of mobile and immobile particles, respectively. The dashed lines mark the mobile- and immobile-particle percolation temperatures defined from the criterion that the LC is 100 times larger than SLC. (h) and (i) do not show the α and α_2 processes because of the uncertainty of their relative positions. The supplementary material gives details of α_2 process and the fitting procedure used.

below which the mobile and immobile-particle percolations are well enough separated for a β relaxation to be identifiable, which is not the case above the threshold.

Figure 4 illustrates our results by showing representative loss spectra in a plot where the x coordinate is the ratio of the two percolation temperatures and the y coordinate is the probe frequency. There is a pronounced β process at long time scales and at a low ratio of the percolation temperatures (lower left corner). When the β process is close to the α process ($T_{P_m}/T_{P_{im}} > 0.85$), it is seen manifested only as an excess wing even at low probe frequencies.

Our results unambiguously link the $G(\omega)$ linear-response properties to double percolation. We have entirely analogous results for the dynamic Young's modulus $E(\omega)$ (not shown).

To critically test the double-percolation scenario, we also simulated systems in 2d where one cannot at the same time have percolation of both the mobile and the immobile particles: If one type of particles percolate, their percolation cluster will necessarily sever any infinite cluster of the opposite kind of particles (think of the paths and walls of a labyrinth – if the walls percolate, the paths do not, and *vice versa*). Thus according

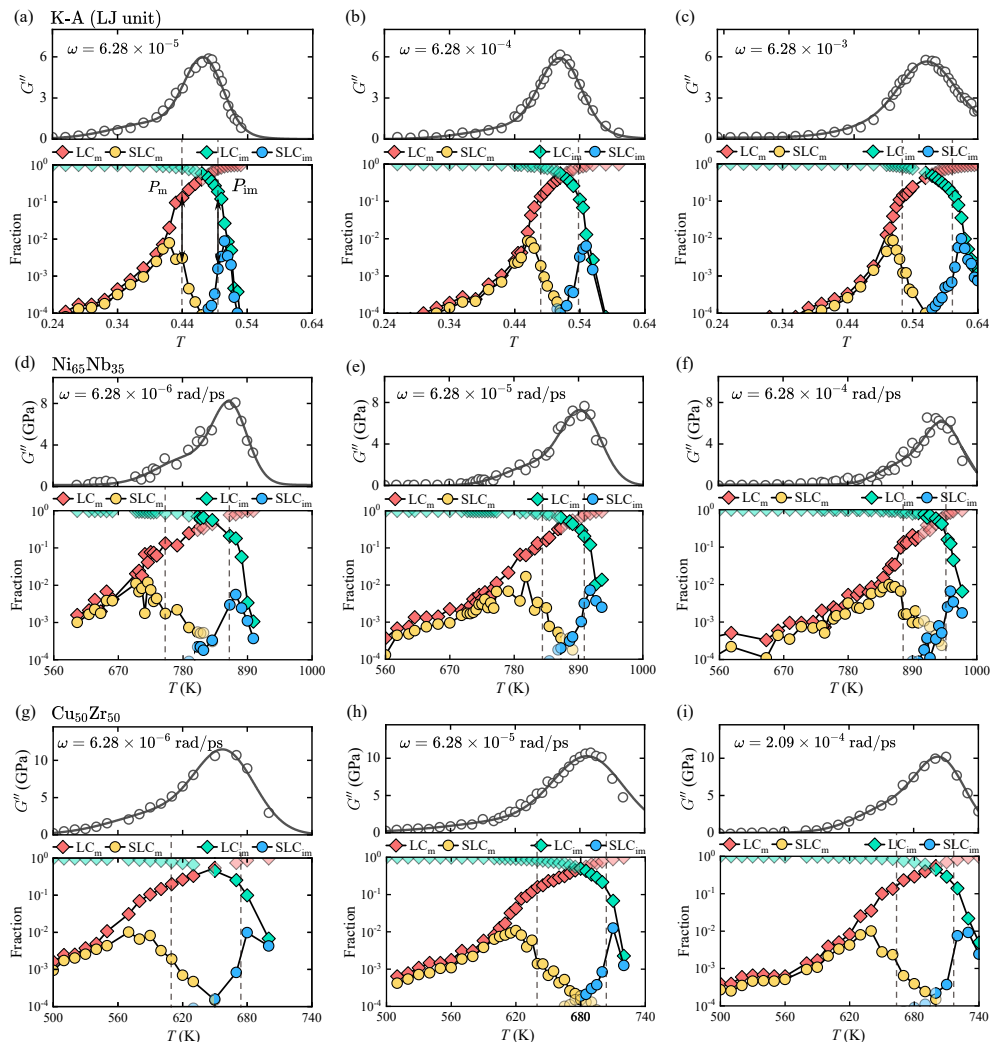


FIG. 3. Double-percolation cluster analysis of 65:35 Kob-Andersen (K-A), $\text{Ni}_{65}\text{Nb}_{35}$, and $\text{Cu}_{50}\text{Zr}_{50}$ mixtures at different frequencies. The upper panels display $G''(\omega)$ for samples cooled at rate $2 \cdot 10^{-7}$ (K-A, LJ units) and 0.1 K/ns ($\text{Ni}_{65}\text{Nb}_{35}$ and $\text{Cu}_{50}\text{Zr}_{50}$). As in Fig. 2 all systems have the α process at the immobile-particle percolation temperature, whereas in contrast to Fig. 2 these three samples have no well-defined β processes at the mobile-particle percolation threshold.

to the double-percolation scenario no separate α and β processes should exist in 2d, and the ratio of the two percolation temperatures should be close to unity. This is tested for three systems in Figure 5. In no cases do we find a β process, and the ratio of the two percolation temperatures is indeed always significantly above 0.85; in fact it is slightly above unity.

Because each of the two percolation temperatures is defined by reference to the specific time scale $\Delta t = 2\pi/\omega$, repeating the simulations for different frequencies allows one to identify the two time scale's temperature dependencies. Results for these are shown for four systems in Fig. 6 for frequencies covering slightly more than 1.5 decade, a figure that also plots the α and β loss-maximum temperatures at the corresponding frequencies. Within the numerical uncertainty the latter coincide with the immobile- and mobile-percolation temperatures, respec-

tively. This confirms the connection between double percolation and mechanical response.

III. CONCLUSION

Percolation is important in many contexts involving disordered solids [68] by determining, e.g., thermodynamics, fragility, and stability of chalcogenide glasses [69, 70], ac conduction at extreme disorder [71], spatial heterogeneity of soft modes [72], vibrational anomalies [73], yielding [74], etc. This paper has investigated numerically a scenario according to which percolation also controls the two main relaxation processes of glass-forming liquids. Extensive computer simulations of binary systems in two and three dimensions establish the following. Two temperatures can be identified mark-

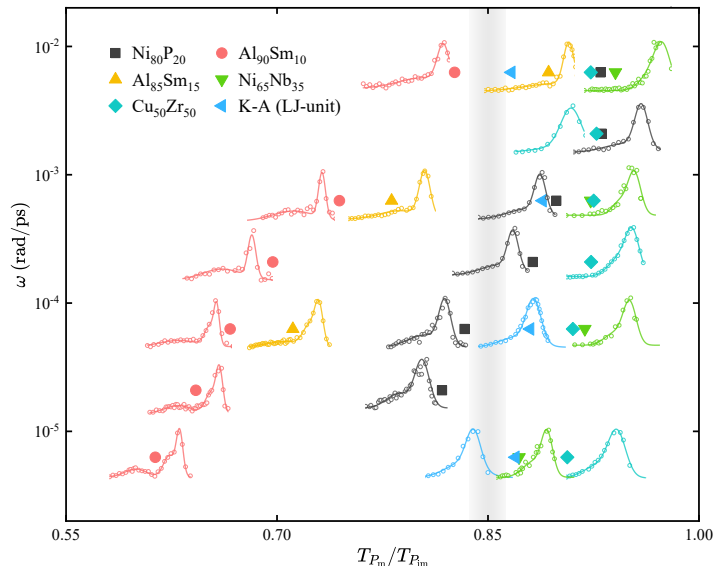


FIG. 4. The ratio between mobile and immobile percolation temperatures determines the β process manifestation. The figure shows selected loss spectra for 3d mixtures at different frequencies. At low frequencies and small percolation-temperature ratio, a pronounced β process is observed: When the ratio is below roughly 0.85 (marked in grey), the β process is a “shoulder” or a “peak”, while it is at most an “excess wing” at larger percolation-temperature ratios.

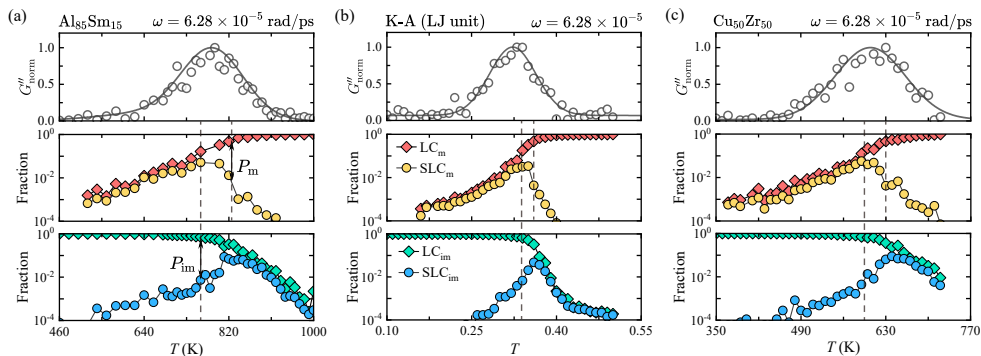


FIG. 5. Double-percolation cluster analysis of 2d models. (a) gives data for the $\text{Al}_{85}\text{Sm}_{15}$ mixture, (b) for the Kob-Andersen mixture, and (c) for the $\text{Cu}_{50}\text{Zr}_{50}$ mixture. Contrary to in 3d, the two percolation processes take place at close temperatures. This is consistent with the finding that there are no separate α and β processes (upper panels): in 2d mobile and immobile-particle percolation cannot occur at the same time.

ing the percolation of mobile and immobile particles, respectively, defined by reference to particle displacements on a specific time scale. One percolation temperature marks the immobile-particle percolation threshold found above the glass transition temperature, another marks the mobile-particle percolation taking place in the glass. Whenever the two percolation temperatures are well separated, they pinpoint the α and β shear-modulus loss-peak temperatures of the frequency corresponding to the time scale in question. A ratio of approximately 0.85 of the two percolation temperatures separates the two cases; below this threshold the α and β processes are well separated, above it they are partly or fully merged. In two

dimensions, where one cannot have both percolation of mobile and immobile particles at the same time, there are no separate α and β processes – here the ratio of the two percolation temperatures is close to unity, in fact slightly above.

We have found no exceptions to this connection between percolation and linear-response properties. More work is needed, however, before generality of the double-percolation picture can be concluded. In particular, it will be important to simulate more complex systems like molecular and polymer glass formers to investigate whether percolation also here controls the α and β processes.

TABLE I. Data of Fig. 2 and Fig. 3, demonstrating that how well separated the β process is from the α process correlates with the ratio between the mobile- and the immobile-particle percolation temperatures. How the β manifestation is arrived at is detailed in Fig S7 of the supplementary material.

	ω (rad/ps)	T_{P_m} (K)	$T_{P_{im}}$ (K)	$T_{P_m}/T_{P_{im}}$	β manifestation
Ni ₈₀ P ₂₀	2.09×10^{-5}	425	520	0.82	Shoulder
	6.28×10^{-5}	450	540	0.83	Shoulder
	2.09×10^{-4}	485	550	0.88	Excess wing
	6.28×10^{-4}	505	562	0.90	Excess wing
	2.09×10^{-3}	538	578	0.93	Excess wing
	6.28×10^{-3}	558	600	0.93	Excess wing
Al ₉₀ Sm ₁₀	6.28×10^{-6}	365	595	0.61	Peak
	2.09×10^{-5}	395	615	0.64	Peak
	6.28×10^{-5}	422	633	0.67	Peak
	2.09×10^{-4}	460	660	0.70	Peak
	6.28×10^{-4}	495	665	0.74	Peak
	6.28×10^{-3}	585	708	0.83	Shoulder
Al ₈₅ Sm ₁₅	6.28×10^{-5}	505	710	0.71	Peak
	6.28×10^{-4}	590	755	0.79	Shoulder
	6.28×10^{-3}	710	795	0.89	Excess wing
Ni ₆₅ Nb ₃₅	6.28×10^{-6}	750	860	0.87	Excess wing
	6.28×10^{-5}	827	900	0.92	Excess wing
	6.28×10^{-4}	875	948	0.92	Excess wing
	6.28×10^{-3}	950	1010	0.94	Excess wing
Cu ₅₀ Zr ₅₀	6.28×10^{-6}	610	673	0.91	Excess wing
	6.28×10^{-5}	640	703	0.91	Excess wing
	2.09×10^{-4}	662	717	0.92	Excess wing
	6.28×10^{-4}	680	735	0.93	Excess wing
	2.09×10^{-3}	700	755	0.93	Excess wing
	6.28×10^{-3}	720	780	0.92	Excess wing
K-A (LJ-unit)	6.28×10^{-6}	0.40	0.46	0.87	Excess wing
	6.28×10^{-5}	0.44	0.50	0.88	Excess wing
	6.28×10^{-4}	0.48	0.54	0.89	Excess wing
	6.28×10^{-3}	0.52	0.60	0.87	Excess wing

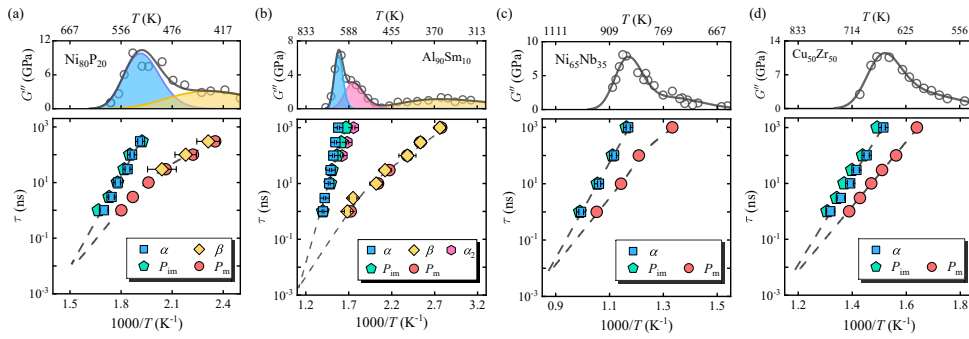


FIG. 6. Temperature dependence of the α and β processes and of the mobile- and immobile-particle percolation times for (a) Ni₈₀P₂₀, (b) Al₉₀Sm₁₀, (c) Ni₆₅Nb₃₅, (d) Cu₅₀Zr₅₀. The upper panels show examples of the loss moduli at a fixed frequency. For Ni₆₅Nb₃₅ and Cu₅₀Zr₅₀, the α and β processes are not well separated, for Al₉₀Sm₁₀ there is an additional α_2 -process reflecting the asymmetry of the α process (pink hexagon in the lower panel). The lower panels plot the percolation time scales and relaxation times. The α and α_2 processes (blue square) give the temperature dependence of the average relaxation time (inverse loss-peak frequency), which is the same as that of immobile-particle percolation (green pentagon). Likewise, the β process (yellow diamond) has the same temperature dependence of its average relaxation time as that of the mobile-particle percolation (orange circle). The dashed lines are guides to the eye illustrating how the two processes merge at high temperatures.

IV. METHODS

Molecular Dynamics simulations and dynamic mechanical spectroscopy

Nine different mixtures were simulated using LAMMPS [75]. The 3d mixtures are: Ni₈₀P₂₀, Al₉₀Sm₁₀, Al₈₅Sm₁₅, Ni₆₅Nb₃₅, Cu₅₀Zr₅₀, and 65:35 Kob-Andersen, the 2d mixtures are Al₈₅Sm₁₅, Cu₅₀Zr₅₀, and 65:35 Kob-Andersen. With the exception of the Kob-Andersen mixtures, which use Lennard-Jones pair potentials, all mixtures employ the embedded atom method (EAM) potential [76]. Simulations are initiated using the melt-quench method, which involves two steps: 1) annealing the mixture at a high temperature above the melting point until its energy stabilizes, thus producing a high-temperature equilibrium liquid; 2) cooling of this liquid to below room temperature (the final temperature of the Kob-Andersen mixtures is below 0.2). The time step of the annealing is 1 fs and of the cooling 2 fs (0.001 and 0.002 for Kob-Andersen mixtures, respectively). The simulations employ periodic boundary conditions, Nose-Hoover thermostat, and were performed in the NPT ensemble (2d mixtures and the 3d Kob-Anderson mixture use NVT ensembles).

Our Molecular Dynamics simulations numerically mimic the protocol of real DMS experiments. An NVT ensemble is used and a sinusoidal volume-preserving strain $\varepsilon(t) = \varepsilon_0 \sin(\omega t)$ is applied at selected times with strain amplitude ε along the x or xy direction of the simulation box. The resulting shear stress σ is fitted by $\sigma(t) = \sigma_0 \sin(\omega t + \delta)$, i.e., has a phase difference δ compared to the strain ε . The storage and loss moduli are calculated from $G' = \sigma_0/\varepsilon_0 \cos(\delta)$ and $G'' = \sigma_0/\varepsilon_0 \sin(\delta)$, respectively. The deformation amplitude ε_0 should be small enough to be within the linear-response regime. To strike a balance between system stability and simulation duration, a time step of 10 fs is utilized. Table S1 of the Supplement summarizes the details of the molecular

dynamics simulations.

Cluster and percolation analysis

The double-percolation scenario divides the particles into two classes, mobile and immobile, depending on the magnitude of the displacement u of the particles over one MD-DMS cycle. In order to identify a suitable critical displacement, u_c , to distinguish between mobile and immobile particles, the van Hove function $p(u) \equiv [P(u + \Delta u) - P(u)]/\Delta u$ is used in which $P(u)$ is the cumulative distribution quantifying the probability of finding the value $X \leq u$ (normalized according to $\int_0^\infty p(u) du = P(\infty) = 1$). u_c is defined from the first minimum of $p(u)$; by definition all mobile particles thus have a displacements greater than u_c . A cluster consists of particles “close” to their neighbors, which is defined by reference to the all-particle radial distribution function $g(r)$. When the distance between particles is below that marking the first minimum of $g(r)$, r_c , particles by definition belong to the same cluster. The values of u_c and r_c depend on the system in question, but for all the systems we find that these values are almost identical at different temperatures and frequencies (Figure. S3 of the Supplement). Table S2 of the Supplement reports u_c and r_c for all mixtures.

A sequence of clusters with varying sizes (number of particles) can be identified based on u_c and r_c . The largest cluster is denoted as LC, the second largest cluster as SLC. The criterion applied to determine the two percolation temperatures T_{P_m} and $T_{P_{im}}$ is that the size of LC is 100 times that of SLC.

ACKNOWLEDGMENTS

The computational work was carried out on the public computing service platform provided by the Network and Computing Center of HUST. We thank for the support from the National Science Foundation of China 52071147. This work was also supported by the VILLUM Foundation’s *Matter* grant VIL16515.

-
- [1] G. Harrison, *The Dynamic Properties of Supercooled Liquids* (Academic, New York, 1976).
 - [2] C. A. Angell, Formation of glasses from liquids and biopolymers, *Science* **267**, 1924 (1995).
 - [3] M. D. Ediger, C. A. Angell, and S. R. Nagel, Supercooled liquids and glasses, *J. Phys. Chem* **100**, 13200 (1996).
 - [4] P. G. Debenedetti and F. H. Stillinger, Supercooled liquids and the glass transition, *Nature* **410**, 259 (2001).
 - [5] J. C. Dyre, The glass transition and elastic models of glass-forming liquids, *Rev. Mod. Phys.* **78**, 953 (2006).
 - [6] L. Berthier and G. Biroli, Theoretical perspective on the glass transition and amorphous materials, *Rev. Mod. Phys.* **83**, 587 (2011).
 - [7] G. L. Hunter and E. R. Weeks, The physics of the colloidal glass transition, *Rep. Prog. Phys.* **75**, 066501 (2012).
 - [8] W. H. Wang, The elastic properties, elastic models and elastic perspectives of metallic glasses, *Prog. Mater. Sci.* **57**, 487 (2012).
 - [9] G. B. McKenna and S. L. Simon, 50th anniversary perspective: Challenges in the dynamics and kinetics of glass-forming polymers, *Macromolecules* **50**, 6333 (2017).
 - [10] C. Alba-Simionesco and G. Tarjus, A perspective on the fragility of glass-forming liquids, *J. Non-Cryst. Solids X* **14**, 100100 (2022).
 - [11] T. Hecksher, A. I. Nielsen, N. B. Olsen, and J. C. Dyre, Little evidence for dynamic divergences in ultraviscous molecular liquids, *Nat. Phys.* **4**, 737 (2008).
 - [12] J. Lamb, Viscoelasticity and lubrication: A review of liquid properties, *J. Rheol.* **22**, 317 (1978).
 - [13] N. G. McCrum, B. E. Read, and G. Williams, *Anelastic and dielectric effects in polymeric solids* (Wiley, 1967).

- [Dover edition, 1991]).
- [14] N. B. Olsen, J. C. Dyre, and T. Christensen, Structural relaxation monitored by instantaneous shear modulus, *Phys. Rev. Lett.* **81**, 1031 (1998).
- [15] F. Kremer and A. Schönhal, eds., *Broadband Dielectric Spectroscopy* (Springer, 2003).
- [16] H. B. Yu, W. H. Wang, H. Y. Bai, and K. Samwer, The β -relaxation in metallic glasses, *Natl. Sci. Rev.* **1**, 429 (2014).
- [17] R. Richert, Supercooled liquids and glasses by dielectric relaxation spectroscopy, *Adv. Chem. Phys.* **156**, 101 (2015).
- [18] G. P. Johari and M. Goldstein, Viscous liquids and the glass transition. II. Secondary relaxations in glasses of rigid molecules, *J. Chem. Phys.* **53**, 2372 (1970).
- [19] M. Goldstein, Viscous liquids and the glass transition: A potential energy barrier picture, *J. Chem. Phys.* **51**, 3728 (1969).
- [20] L. Berthier, G. Biroli, J.-P. Bouchaud, L. Cipelletti, and W. van Saarloos, eds., *Dynamical Heterogeneities in Glasses, Colloids, and Granular Media* (Oxford Univ. Press, 2011).
- [21] S. Karmakar, C. Dasgupta, and S. Sastry, Growing length scales and their relation to timescales in glass-forming liquids, *Annu. Rev. Cond. Mat. Phys.* **5**, 255 (2014).
- [22] Q. Yang, C.-Q. Pei, H.-B. Yu, and T. Feng, Metallic nanoglasses with promoted β -relaxation and tensile plasticity, *Nano Letters* **21**, 6051 (2021), pMID: 34240612, <https://doi.org/10.1021/acs.nanolett.1c01283>.
- [23] K. L. Ngai, R. Casalini, S. Capaccioli, M. Paluch, and C. M. Roland, Do theories of the glass transition, in which the structural relaxation time does not define the dispersion of the structural relaxation, need revision?, *J. Phys. Chem. B* **109**, 17356 (2005).
- [24] K. L. Ngai, J. Habasaki, D. Prevosto, S. Capaccioli, and M. Paluch, Thermodynamic Scaling of α -Relaxation Time and Viscosity Stems from the Johari-Goldstein β -Relaxation or the Primitive Relaxation of the Coupling Model, *J. Chem. Phys.* **137**, 034511 (2012).
- [25] K. Ngai, Universal properties of relaxation and diffusion in complex materials: Originating from fundamental physics with rich applications, *Progress in Materials Science* **139**, 101130 (2023).
- [26] A. Kudlik, S. Benkhof, T. Blochowicz, C. Tschirwitz, and E. Rössler, The dielectric response of simple organic glass formers, *J. Mol. Struct.* **479**, 201 (1999).
- [27] W. Götze, *Complex dynamics of glass-forming liquids: A mode-coupling theory* (Oxford University Press, 2008).
- [28] S. Kaufmann, S. Wefing, D. Schaefer, and H. W. Spiess, Two-dimensional exchange nuclear magnetic resonance of powder samples. III. Transition to motional averaging and application to the glass transition, *J. Chem. Phys.* **93**, 197 (1990).
- [29] A. Arbe, D. Richter, J. Colmenero, and B. Farago, Merging of the α and β relaxations in polybutadiene: A neutron spin echo and dielectric study, *Phys. Rev. E* **54**, 3853 (1996).
- [30] N. B. Olsen, Scaling of β -relaxation in the equilibrium liquid state of sorbitol, *J. Non-Cryst. Solids* **235**, 399 (1998).
- [31] U. Schneider, R. Brand, P. Lunkenheimer, and A. Loidl, Excess wing in the dielectric loss of glass formers: A Johari-Goldstein β relaxation?, *Phys. Rev. Lett.* **84**, 5560 (2000).
- [32] C. Scalliet, B. Guiselin, and L. Berthier, Excess wings and asymmetric relaxation spectra in a facilitated trap model, *J. Chem. Phys.* **155**, 064505 (2021).
- [33] B. Guiselin, C. Scalliet, and L. Berthier, Microscopic origin of excess wings in relaxation spectra of supercooled liquids, *Nat. Phys.* **18**, 468 (2022).
- [34] J. C. Dyre and N. B. Olsen, Minimal model for beta relaxation in viscous liquids, *Phys. Rev. Lett.* **91**, 155703 (2003).
- [35] P. G. Wolyne, Randomness and complexity in chemical physics, *Acc. Chem. Res.* **25**, 513 (1992).
- [36] S. R. Broadbent and J. M. Hammersley, Percolation processes: I. Crystals and mazes, *Math. Proc. Camb. Philos. Soc.* **53**, 629 (1957).
- [37] D. Stauffer and A. Aharony, *Introduction To Percolation Theory*, 2nd ed. (Routledge, 1992).
- [38] G. Grimmett, *Percolation*, 2nd ed. (Springer, 1999).
- [39] M. B. Isichenko, Percolation, statistical topography, and transport in random media, *Rev. Mod. Phys.* **64**, 961 (1992).
- [40] J. C. Dyre, *Solid-that-flows* picture of glass-forming liquids, *J. Phys. Chem. Lett.* **15**, 1603 (2024).
- [41] G. Diezemann, A free-energy landscape model for primary relaxation in glass-forming liquids: Rotations and dynamic heterogeneities, *J. Chem. Phys.* **107**, 10112 (1997).
- [42] H. Sillescu, Heterogeneity at the glass transition: a review, *J. Non-Cryst. Solids* **243**, 81 (1999).
- [43] G. H. Fredrickson and H. C. Andersen, Kinetic Ising model of the glass transition, *Phys. Rev. Lett.* **53**, 1244 (1984).
- [44] J. P. Garrahan and D. Chandler, Geometrical explanation and scaling of dynamical heterogeneities in glass forming systems, *Phys. Rev. Lett.* **89**, 035704 (2002).
- [45] F. Ritort and P. Sollich, Glassy dynamics of kinetically constrained models, *Adv. Phys.* **52**, 219 (2003).
- [46] R. N. Chacko, F. P. Landes, G. Biroli, O. Dauchot, A. J. Liu, and D. R. Reichman, Elastoplasticity mediates dynamical heterogeneity below the mode coupling temperature, *Phys. Rev. Lett.* **127**, 048002 (2021).
- [47] G. Zhang, H. Xiao, E. Yang, J. S. Robert, S. A. Ridout, R. A. Riggleman, D. J. Durian, and A. J. Liu, Structuro-elasto-plasticity model for large deformation of disordered solids, *Phys. Rev. Res.* **4**, 043026 (2022).
- [48] M. Ozawa and G. Biroli, Elasticity, facilitation, and dynamic heterogeneity in glass-forming liquids, *Phys. Rev. Lett.* **130**, 138201 (2023).
- [49] L. Costigliola, T. Hecksher, and J. C. Dyre, Glass-forming liquids need facilitation, *PNAS* **121**, e2408798121 (2024).
- [50] J. D. Stevenson and P. G. Wolyne, A universal origin for secondary relaxations in supercooled liquids and structural glasses, *Nat. Phys.* **6**, 62 (2010).
- [51] L. Gao, Y. Sun, and H.-B. Yu, Mobility percolation as a source of Johari-Goldstein relaxation in glasses, *Phys. Rev. B* **108**, 014201 (2023).
- [52] C. Donati, J. F. Douglas, W. Kob, S. J. Plimpton, P. H. Poole, and S. C. Glotzer, Stringlike cooperative motion in a supercooled liquid, *Phys. Rev. Lett.* **80**, 2338 (1998).
- [53] M. Russina, F. Mezei, R. Lechner, S. Longeville, and B. Urban, Experimental evidence for fast heterogeneous collective structural relaxation in a supercooled liquid near the glass transition, *Phys. Rev. Lett.* **84**, 3630 (2000).

- [54] D. Long and F. Lequeux, Heterogeneous dynamics at the glass transition in van der Waals liquids, in the bulk and in thin films, *Eur. Phys. J. E* **4**, 371 (2001).
- [55] Y. Shi and M. L. Falk, Strain localization and percolation of stable structure in amorphous solids, *Phys. Rev. Lett.* **95**, 095502 (2005).
- [56] F. W. Starr, J. F. Douglas, and S. Sastry, The relationship of dynamical heterogeneity to the Adam-Gibbs and random first-order transition theories of glass formation, *J. Chem. Phys.* **138**, 12A541 (2013).
- [57] M. T. Cicerone, Q. Zhong, and M. Tyagi, Picosecond dynamic heterogeneity, hopping, and Johari-Goldstein relaxation in glass-forming liquids, *Phys. Rev. Lett.* **113**, 117801 (2014).
- [58] H.-B. Yu, R. Richert, and K. Samwer, Structural rearrangements governing Johari-Goldstein relaxations in metallic glasses, *Sci. Adv.* **3**, e1701577 (2017).
- [59] B. A. P. Betancourt, F. W. Starr, and J. F. Douglas, String-like collective motion in the α - and β -relaxation of a coarse-grained polymer melt, *J. Chem. Phys.* **148**, 104508 (2018).
- [60] F. Caporaletti, S. Capaccioli, S. Valenti, M. Mikolasek, A. I. Chumakov, and G. Monaco, A microscopic look at the Johari-Goldstein relaxation in a hydrogen-bonded glass-former, *Sci. Rep.* **9**, 14319 (2019).
- [61] F. Caporaletti, S. Capaccioli, S. Valenti, M. Mikolasek, A. I. Chumakov, and G. Monaco, Experimental evidence of mosaic structure in strongly supercooled molecular liquids, *Nat. Commun.* **12**, 1867 (2021).
- [62] C. Chang, H. P. Zhang, R. Zhao, F. C. Li, P. Luo, M. Z. Li, and H. Y. Bai, Liquid-like atoms in dense-packed solid glasses, *Nat. Mater.* **21**, 1240 (2022).
- [63] I. M. Douglass and J. C. Dyre, Distance-as-time in physical aging, *Phys. Rev. E* **106**, 054615 (2022).
- [64] F. Spieckermann, D. Söpu, V. Soprunyuk, M. B. Kerber, J. Bednarcik, A. Schökel, A. Rezvan, S. Ketov, B. Sarac, E. Schaffer, and J. Eckert, Structure-dynamics relationships in cryogenically deformed bulk metallic glass, *Nat. Commun.* **13**, 127 (2022).
- [65] V. N. Novikov, E. Rössler, V. K. Malinovsky, and N. V. Surovtsev, Strong and fragile liquids in percolation approach to the glass transition, *Europhys. Lett.* **35**, 289 (1996).
- [66] D. M. Heyes and J. R. Melrose, Percolation cluster statistics of Lennard-Jones fluids, *Mol. Phys.* **66**, 1057 (1989).
- [67] W. Kob and H. C. Andersen, Testing mode-coupling theory for a supercooled binary Lennard-Jones mixture I: The van Hove correlation function, *Phys. Rev. E* **51**, 4626 (1995).
- [68] A. Zaccone, *Theory of disordered solids* (Springer, 2023).
- [69] J. C. Phillips and M. F. Thorpe, Constraint theory, vector percolation and glass formation, *Solid State Commun.* **53**, 699 (1985).
- [70] M. Tatsumisago, B. L. Halfpap, J. L. Green, S. M. Lindsay, and C. A. Angell, Fragility of Ge-As-Se glass-forming liquids in relation to rigidity percolation, and the Kauzmann paradox, *Phys. Rev. Lett.* **64**, 1549 (1990).
- [71] T. B. Schröder and J. C. Dyre, ac hopping conduction at extreme disorder takes place on the percolating cluster, *Phys. Rev. Lett.* **101**, 025901 (2008).
- [72] V. K. d. Souza and P. Harrowell, Rigidity percolation and the spatial heterogeneity of soft modes in disordered materials, *PNAS* **106**, 15136 (2009).
- [73] A. Marruzzo, S. Köhler, A. Fratallocchi, G. Ruocco, and W. Schirmacher, Vibrational anomalies and marginal stability of glasses, *Eur. Phys. J. Spec. Top.* **216**, 83 (2013).
- [74] A. Ghosh, Z. Budrikis, V. Chikkadi, A. L. Sellar, S. Zapperi, and P. Schall, Direct observation of percolation in the yielding transition of colloidal glasses, *Phys. Rev. Lett.* **118**, 148001 (2017).
- [75] A. P. Thompson, H. M. Aktulga, R. Berger, D. S. Bolintineanu, W. M. Brown, P. S. Crozier, P. J. in 't Veld, A. Kohlmeyer, S. G. Moore, T. D. Nguyen, R. Shan, M. J. Stevens, J. Tranchida, C. Trott, and S. J. Plimpton, LAMMPS - a flexible simulation tool for particle-based materials modeling at the atomic, meso, and continuum scales, *Computer Physics Communications* **271**, 108171 (2022).
- [76] W. M. Brown and M. Yamada, Implementing molecular dynamics on hybrid high performance computers—three-body potentials, *Computer Physics Communications* **184**, 2785 (2013).